Manganese as Fuel in Slow-Burning Pyrotechnic Time Delay Compositions

Darren Swanepoel[1], Olinto Del Fabbro[1] and Walter W. Focke[1*]

[1]Institute of Applied Materials, Department of Chemical Engineering, University of Pretoria, Lynnwood Road, Pretoria, South Africa

Corrie Conradie[2†]

[2]Research and Technology, African Explosives Limited, PO Modderfontein, 1645, South Africa

Abstract

Manganese metal was evaluated as a fuel for slow-burning delay compositions press-filled in aluminium or compaction-rolled in lead tubes. Oxides of antimony, bismuth, copper, manganese and vanadium were considered as oxidants. Measured burn rates for binary mixtures varied between 5 and 22 mm/s but slower burning ternary and quaternary compositions were also found. The addition of fumed silica to the Mn/MnO_2 system had little effect on the propagation rate but a low level addition of hollow glass sphere significantly reduced the burn rate. $Mn - MnO_2$ mixtures showed reliable burning over a wide stoichiometric range. In this system the fuel and the oxidant share a common metal. They combine to form the more stable intermediate oxide (MnO) releasing considerable quantities of heat in the process.

Keywords: Pyrotechnics, Time delay, Manganese, Antimony oxide, Fumed silica

1 Introduction

Commercial detonator delay element assemblies comprise an ignition source, a small-diameter tube containing a compacted pyrotechnic composition and an ignition transfer system [1, 2]. The pyrotechnic composition is a mixture of an oxidising agent and a fuel capable of an exothermic redox reaction. Following ignition, a combustion wave travels down along the tube at a constant velocity. This ensures the transmission of the initiation impulse to the detonator in a precisely adjustable time interval. The actual time delay is determined by the nature of the reactants and the stoichiometry of the pyrotechnic composition, the dimensions of the column, i.e. its length and diameter, and the material of construction of the tube [2].

The reaction must be exothermic, self-sustained and self-contained [3]. Preferred delay compositions ought to burn in an essentially gasless fashion (volume of gas evolved less than

* Corresponding author; e-mail: walter.focke@up.ac.za

† In memoriam

100 L/kg of mixture [4]) and at a constant predetermined rate. Current pyrotechnic time delay formulations are based on silicon as fuel in combination with red lead oxide (fast burning for short-time delays) or barium sulphate (slow burning for long-time delays).

The combustion event in the column is governed by a number of parameters. The thermal diffusivity of the mixture is important as wave propagation depends on repeated re-ignition of adjacent layers along the burning path. Good mixing and adequate particle-particle contact between reactants is a prerequisite for stable and reproducible burning owing to the low values of the diffusion coefficients. The simplest theory [5] relates the burning rate to the physical properties of the mixture. It assumes composition- and temperature-independent physical properties, a thin reaction zone and a gasless exothermic n^{th} order solid-state reaction with Arrhenius-type temperature dependence for the rate constant:

$$k = k_o e^{E/RT} \tag{1}$$

It yields the following expression for the linear burn rate:

$$u = \sqrt{\frac{\lambda k_o R T_c^2}{\rho E \Delta H_R g(n)} e^{E/RT_c}} \tag{2}$$

Here u is the burn rate in m/s, λ is the thermal conductivity in W/m.K; ρ is the density in kg/m^3; R is the gas constant (8.314 J/mol.K); T_c is the maximum temperature of the burning column; E is the apparent Arrhenius activation energy in J/mol; ΔH_R is the heat of reaction in J/kg; k and k_o are the rate constant and Arrhenius pre-exponential factor in m/s, and $g(n)$ is a weak function of the reaction order n that varies between 1 and 2.

Equation (2) suggests that a slow burn rate requires a composition that releases a large amount of heat at a slow rate to sustain the thermal wave of reaction. It also identifies the combustion wave temperature, T_c, as the most significant variable affecting burn rate. Adjusting stoichiometry and the addition of inert substances can control it. The temperature of the wave front is also affected by transverse heat losses and hence by the nature of material used for tube construction. The rolled lead tubes used in current delay elements will be soon be replaced by rigid aluminium tubes. Unfortunately the slow burning pyrotechnic mixtures used in long-time delays show variable burn performance in aluminium.

This purpose of this study was to identify slow burning compositions (burn rate < 5 mm/s) with reliable ignition and burn behaviour in rigid aluminium tubes. Manganese was chosen as fuel because the metal powder is available as a waste product from a manganese ore processing plant.

2 Experimental

2.1 Materials

Manganese [CAS No. 7439-96-5] powder was obtained from Manganese Metal Company (MMC). The particle size of this waste product ranged from few micrometers to fractions of a millimetre. The larger fraction was removed by sieving. The sieved material was milled in a tungsten ball mill for twelve hours. The volumetric mean particle size (d_{50}) of the resultant

milled powder was 6.0 μm; the surface weighted mean particle size was 13.2 μm and the BET surface area 0.60 m^2/g.

Manganese(IV) oxide [CAS No. 1313-13-9] was supplied by Delta EMD. The material was milled in a roller mill to particle size d_{50} = 10 μm. Vanadium(V) oxide (V_2O_5) [CAS No. 1314-62-1] was obtained from the Rhombus vanadium mine and used as is. The copper(II) oxide [CAS No. 1317-38-0] (CuO) and the copper(I) oxide [CAS No. 1317-39-1] (Cu_2O) were both obtained from Sigma-Aldrich. These laboratory grade materials were milled into fine powders using a ball mill.

Sb_6O_{13} [CAS No. 12165-47-8] was synthesized according to the procedure described by Kalombo *et al.* [6]. Dry colloidal antimony pentoxide [CAS No. 1314-60-9] purchased from Nyacol® Nano Technologies was placed in a crucible and covered with a steel lid with a small hole to allow gases to escape. It was then subjected to an 8-hour thermal treatment at 315°C in a convection oven. Thereafter the product was allowed to cool down slowly back to room temperature inside the furnace.

Bismuth(III) oxide [CAS No. 1304-76-3] (Bi_2O_3) was prepared by thermal decomposition of bismuth(III) subcarbonate [CAS No. 5892-10-4] at 460°C using the method described by Kalombo *et al.* [6]. Copper bismuthate ($CuBi_2O_4$) was produced by sintering a mixture of 40% copper nitrate [CAS No. 19004-19-4] and 60% bismuth nitrate [CAS No. 10035-06-0] at 450ºC for 48 hrs. The identity of the material was confirmed by powder X-ray diffraction. It contained bismuth oxide [CAS No. 1304-76-3] as an impurity.

Hollow glass spheres with a nominal diameter of 75 μm (Ballotini Q-Cel 2106) and fumed silica (Aerosil 200 supplied by Degussa) were employed as inert diluents.

Silicon powder (Millrox Type 4) was used as an additional fuel in multicomponent mixtures. It had a surface weighted mean particle size of 0.91 μm and a BET surface area of 10.1 m^2/g.

2.2 Preparation of mixtures

The required quantities of the different ingredients (fuel, oxidant and additives) were weighed and blended thoroughly in a tumble mixer for 4 hours. Thereafter the mixture was passed gently through a 125μm sieve using a soft brush. This process was repeated using a 53 μm sieve. The purpose of the sieve-brush-mixing operation was to break up same-particle agglomerates and to facilitate intimate mixing of the formulation components. Compositions are reported as percentages of fuel on a mass basis. Inert (non reactive) additives levels are expressed as percentage add-on to the reactive pyrotechnic composition.

2.3 Material Characterisation

Particle size was determined using a Malvern Mastersizer Hydro 2000MY instrument. BET surface areas were measured on a Micromeritics Flowsorb II 2300 instrument.

The purity of reagents was determined using a wavelength-dispersive XRF spectrometer (ARL 9400 XP + XRF). The powders were ground in a tungsten carbide milling vessel and roasted at 1000°C for determination of the loss on ignition (LOI). An organic binder (ethyl cellulose) was used during pelletization of samples.

A TA SDT Q600 simultaneous TG/DSC machine was used for the thermal and gravimetric analysis of Mn, MnO_2 and a 50 wt % mixture. Experiments were performed in a 70 μl alumina crucible with or without lids. The samples were scanned at 30 °C/min in pure oxygen as purge gas.

The combustion products of different compositions in the Mn – MnO_2 system were obtained by burning samples in S-type glass tubes with a 4 mm ϕ internal diameter and a wall thickness of 1 mm. These compositions were ignited using shock-tubes and a proprietary starter composition. The slags obtained from the tubes following combustion were ground into a powder. XRD analysis was performed on a PANalytical X'Pert Pro powder diffractometer with X'Celerator detector and variable divergence- and receiving slits with Mn filtered Fe-Kα radiation (0.193609 nm) operated at 25 kV and 35 mA. The phases were identified using X'Pert Highscore plus software and composition quantified using the Rietveld method (Autoquan Program).

High temperature staged XRD analyses were also conducted on the manganese fuel, the manganese(IV) oxide, and on a 50 wt % mixture of these reactants. The samples were compacted using a load of 100 kg into 4 mm ϕ by 0.5 mm pellets. A 6 mm ϕ sapphire disk was placed between the sample and the platinum heating stage to protect against potential damage owing to the exothermic reactions occurring. Spectra were recorded at the following temperatures were 25°C, 500 °C, 570 °C, 680 °C, 810 °C, and 1150 °C. They were chosen on the basis of the TG/DSC results. The samples were heated at 300 °C/min in a static air atmosphere to the lowest selected measurement temperature and kept there for a few minutes before collecting data. This procedure was repeated proceeding to the next selected temperature. Finally the sample was allowed to cool to 25 °C before the completing a final scan. The high temperature stage comprises a platinum heating strip. It features three characteristic peaks (located at 2θ = 50.5°, 59° and 88.5°) that also show up in the XRD scans presented below. It should be noted that these peak positions shift to lower angles as the temperature increases. These peaks were removed from the recorded spectra to avoid confusion and simplify the interpretation.

2.4 Preparation of Delay Elements

2.4.1 Lead Delay Elements

Lead tubes were prepared by drawing proprietary tube-drawing machine used commercially for the manufacture of delay elements. The powder mixture (ca. 15 g) was poured into a 165 mm long lead tube with an outer diameter of 10.2 mm and an average inner diameter of 6 mm. The composition in the tube was compressed and consolidated by a drawing operation. During each drawing operation, the sealed tube was forced through a hole with a smaller diameter. The drawing direction was reversed after each pass to ensure even compaction. The outer and inner diameters were reduced in ten successive steps down to ca. 6 mm and 3.2 ± 0.1 mm respectively. In this way, good compaction of the powdered delay composition was ensured. The volume fraction solids can be calculated from the known densities of the mixture components and the internal diameter the rolled tube. Using this approach it is estimated that 73 % of the theoretical maximum density (TMD) was reached for the 50 wt % Mn – MnO_2 mixture. The rolled lead tube was then cut to a standard length of 45 mm to form the delay elements. A proprietary pyrotechnic starter composition was used to

facilitate ignition. A short increment of the starter was filled into the top of the core after removing 3 mm of the main composition from the lead tube.

2.4.2 Aluminium Delay Elements

Aluminium delay elements were made by drilling 3.3 mm ϕ holes through aluminium rods (OD 6.2 mm ϕ) cut to a length of 45 mm. These tubes were filled incrementally. The mixture was compacted after adding each increment by inserting a punch and applying controlled compaction pressure that was measured by means of a load-cell device (HBM Komm). It was found that the applied compaction pressure during the filling of the aluminium tubes is a critical factor. For example, the Mn – MnO_2 system was "dead pressed" when compaction loads exceeding 105 MPa were employed. However, at compaction loads between 100 and 105 MPa the material ignited and burned in a satisfactory manner. Consequently, for most of the elements prepared in this way, the pressure was set at approximately 100 MPa. A dwell time of about one second was used before relieving the stress. As for the lead elements, a proprietary pyrotechnic mixture was used as a starter element.

The delay elements were assembled into conventional non-electric detonators. The procedure followed is similar to the one used for the assembly of conventional detonators: Only the actual high explosive charge was left out. The time delay was pushed to the bottom of the detonator sleeve and an anti-static cup was fitted. The shock tube was inserted through a grommet such that it touched the antistatic cup. Finally, the sleeve was sealed by a crimping operation.

A small hole (1.5 mm ϕ) was drilled sideways through the detonator sleeve as well as the time delay element inside. A Pt-Pt 13% Rh thermocouple (type R) with 0.38 mm diameter wires was embedded into the composition via this hole at the bottom end.

2.5 Burn Rate Measurement

The trigger box emits an explosive noise when ignition of shock tube occurs. A sound sensor placed in the box (buffer) was used to record this signal as the starting point for the burn reaction. This signal was transmitted to an electronic system provided with amplification circuits that delivered the required signal as a voltage signal to the computer data acquisition card.

The end of the burn was detected by means of a thermocouple measurement that was also recorded via the computer interface. The thermocouple output was sent via an electronic cold junction compensator to data capture software on an Eagle PC 30F personal computer. The gain of amplification was varied between 100 and 1000. The signal-to-noise ratio was improved by utilising a digital filter. The reaction burn rate was calculated as the ratio of the length of the element and the burn time-interval. The latter was taken as the time difference between the starting signal (sound signal) and the final thermal signal provided by the thermocouple.

3 Results and Discussions

3.1 Burn rates

Figures 1 to 3 show the effect of the nature of the oxidant and the stoichiometry of the pyrotechnic mixture on the linear burning rate. The burn behaviour in pressed aluminium tubes can be summarized as follows. The oxidant Bi_2O_3 provided for the fastest burn rates using manganese as fuel. Sustained burning was observed for fuel contents in the range 40 wt % to 60 wt % in the Mn – Bi_2O_3 system. The burn rate of a 40 wt % Mn – $CuBi_2O_4$ mixture was 9.3 mm/s. The Mn – MnO_2 system burned over a wider composition window. Intermediate burn rates were observed with V_2O_5. Figure 2 shows that the slowest burn rates were achieved using Cu_2O as oxidant. For the range of compositions tested in aluminium tubes, the linear burning rate decreased in the sequence:

$$Bi_2O_3 > CuBi_2O_4 \approx MnO_2 > Cu_2O \approx V_2O_5$$

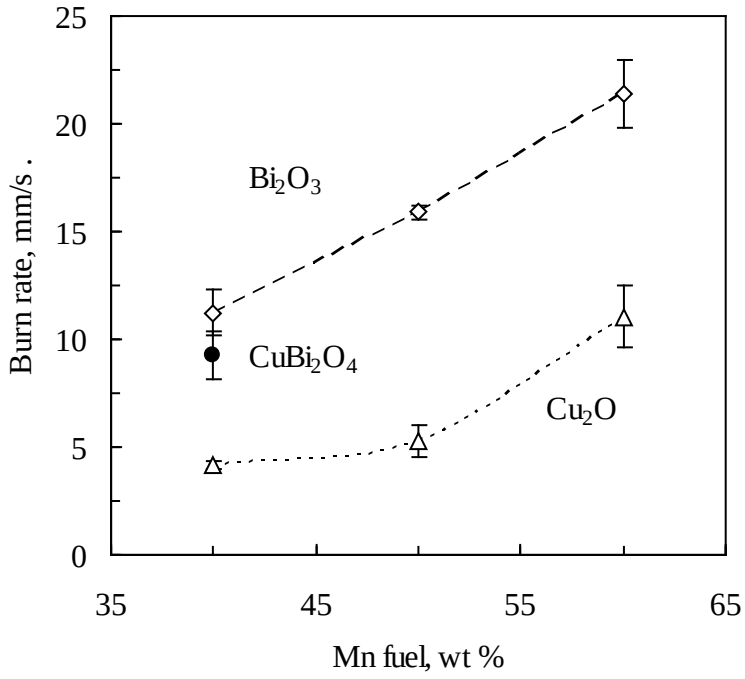

Figure 1. The effect of the oxidants Bi_2O_3, Cu_2O and $CuBi_2O_4$ on burn rate in aluminium tubes.

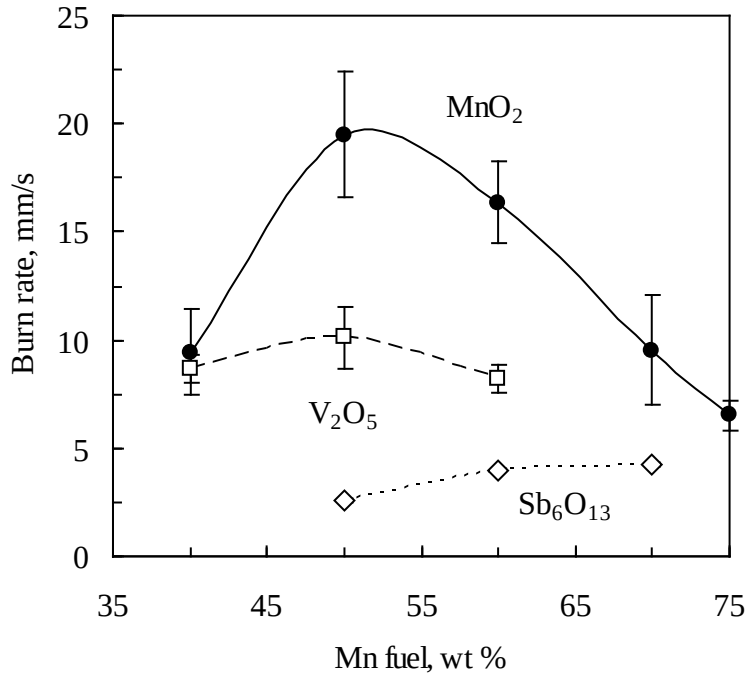

Figure 2. The effect of the oxidants on burn rate. MnO_2- and V_2O_5-based compositions were press-filled in aluminium tubes and Sb_6O_{13} in rolled lead tubes.

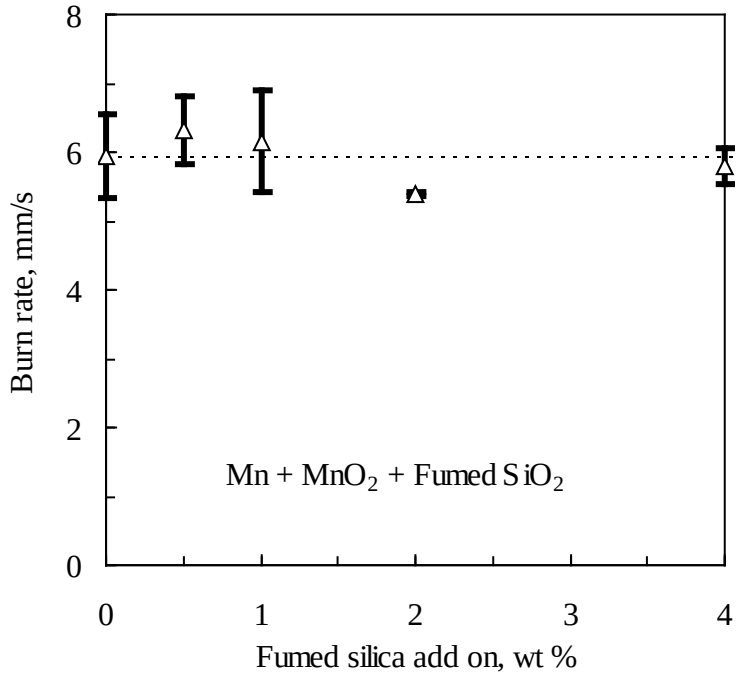

Figure 3. Effect of fumed silica addition on the burn rate of Mn – MnO_2 (38 wt % fuel)

The Mn – Sb_6O_{13} and the Mn – CuO systems were tested in lead tubes. Figure 2 reveals that the Mn – Sb_6O_{13} system featured the lowest recorded burn rates. For Mn – CuO, only the 50 wt % manganese oxide composition burned in a sustained fashion. The average burn rate was 5.5 mm/s. Unfortunately neither system sustained burning in the present aluminium tubes. A previous investigation revealed that Si – Sb_6O_{13} burned at a slower rate in aluminium tubes compared to the lead tubes [6]. These results can be rationalized on the basis of equation (2): The higher thermal conductivity of the aluminium tube wall material results in greater lateral heat losses. This effectively "cools the reaction", i.e. causing the burning to proceed at lower temperature (T_c) and therefore at a slower burn rate. Compared to the faster systems, the slower reactions are more adversely affected by the higher thermal ballast posed by the high thermal conductivity aluminium tube walls.

Unfortunately only the Mn – Cu_2O system provided reliable slow burning (<5 mm/s) performance in aluminium tubes. Next attempts were made to reduce the burn rate of the other systems by adding either inert agents or by considering multicomponent mixtures. Referring to equation (2), the dominant effect of adding inert filler is expected to be the reduction in the apparent heat of the reaction and thus the burn temperature T_c. This means that a lower burn rate is the expected result. However, Figure 3 shows that adding fumed silica to the Mn – MnO_2 system had little effect. Improved mixing of the components obtained in the presence of the silica could have neutralized the effect of adding small amounts of the inert substance [7].

Table 1. Burn rates of ternary compositions.

Composition, wt %						Burn rate	Std. Dev.
Mn	**Si**	**Cu_2O**	**V_2O_5**	**MnO_2**	**Bi_2O_3**	**mm/s**	**mm/s**
40	20	40	-	-	-	8.6	0.7
45	10	45	-	-	-	9.5	1.5
40	20	-	40	-	-	11.9	1.4
72.7	-	-	-	18.2	9.1	5.0	0.9
71.4	-	-	-	23.8	4.8	5.2	1.9

Table 2. Burn rates of quaternary compositions

Composition, Mass %				Burn rate	Std. Dev
Mn	**Sb_6O_{13}**	**CuO**	**Q-Cel**	**mm/s**	**mm/s**
60.34	25.86	8.62	5.17	2.67	0.05
57.85	24.79	12.40	4.96	3.30	0.03

Tables 1 and 2 show additional burn rate results obtained with fuel-rich ternary and quaternary compositions. The first three compositions in Table 1 report on the effect of replacing part of the manganese fuel with silicon as fuel. Invariably the burn rates increased. In the next two mixtures part of the MnO_2 oxidant was substituted with Bi_2O_3. Surprisingly, the burn rates settled down at ca. 5 mm/s. Table 2 shows that slow burning compositions with burn rates less than 4 mm/s can be achieved using ca. 5 wt % hollow glass spheres as diluent

in the ternary system Mn –Sb_6O_{13} – CuO. Note that the CuO was an essential component in latter system as it did not burn in the tube when it was left out.

3.2 Characterisation of the Mn – MnO_2 System

The reliable burning of Mn – MnO_2 compositions was a surprise finding as the fuel and oxidant share a common metal. Well defined manganese dioxide is produced locally in South Africa, primarily for the battery industry. Furthermore, the manganese metal powder used here is a waste product available in sufficient quantities. This implies positive cost implications and it was therefore decided to study and characterize this system in more detail.

The phase behaviour of the Mn – O system has been modelled and reviewed by Wang and Sundman [8] and Grundy et al. [9]. Manganese itself exist in several modifications: α-Mn up to 707 °C, β-Mn up to 1087 °C, γ-Mn up to 1138 °C, and δ-Mn up to the melting temperature of 1246 °C. The stable equilibrium oxide phases are manganosite ($Mn_{1-x}O$), hausmannite (α-Mn_3O_4 transforming to β-Mn_3O_4 above 1177 °C), bixbyite (α-Mn_2O_3 transforming to β- Mn_2O_3 above ~27 °C) and pyrolusite (MnO_2) [9]. There are also several metastable modifications notably the mixed phase (Mn_5O_8) [10, 11]. These multiple possibilities make it difficult to unambiguously characterize the reactions and phase transitions occurring in this system.

3.2.1 Thermochemistry

Figure 4 shows the Ellingham diagram for the various manganese oxides as constructed using the FactSage inorganic thermodynamics program [12]. Such diagrams are a useful tool in the study of pyrotechnic redox reactions. Figure 4 plots the Gibbs free energy of reaction for the following series of normalized manganese oxidation reactions:

Scheme I: $x\,\mathrm{Mn} + \mathrm{O_2} \rightarrow y\,\mathrm{M}_{x/y}\mathrm{O}_{2/y} \quad (x, y) \in \{(1, 1); (4/3, 2/3); (3/2, 1/2); (2, 2)$

As Ellingham [13] noted, the $\Delta G^\circ = \Delta G^\circ(T)$ relationships approximate to straight lines over temperature ranges in which no phase change occurs. The lowest lying line indicates the reaction with the greatest change in the Gibbs free energy, i.e. the one that, thermodynamically, forms the most stable oxide. The Ellingham diagram in Figure 4 indicates that the stability of the various manganese oxides decreases in the following order:

$$MnO > Mn_3O_4 > Mn_2O_3 > MnO_2$$

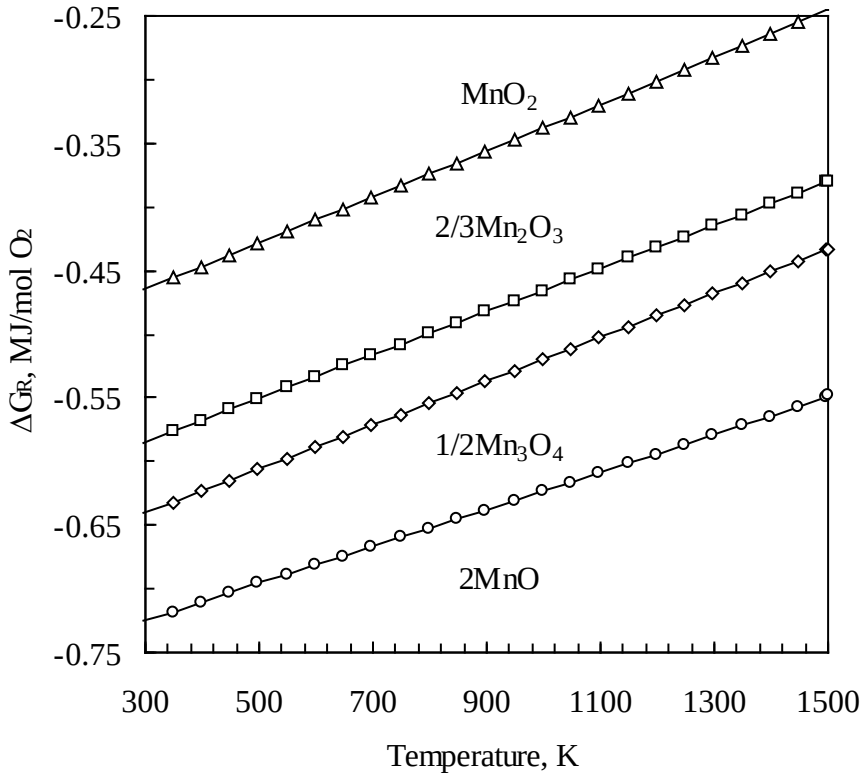

Figure 4. Ellingham diagram for the oxidation reactions of manganese into different oxidation states.

This sequence parallels the increase in the oxidation state of the manganese metal in the corresponding compounds. This implies that the reaction of manganese with a higher oxide will be spontaneous ($\Delta G° < 0$) as a more stable intermediate oxide can be formed as a reaction product. The present study considered the reaction between manganese metal with the thermodynamically least stable manganese(IV) oxide. In this case the lowest oxide that can be formed is MnO, and the second most stable is Mn_3O_4. The reactions required to form these products are shown in Table 3. Also indicated are the stoichiometric compositions as well as the adiabatic reaction temperatures calculated taking phase changes into account. These temperatures far exceed the temperature ranges indicated in the Ellingham diagram in Figure 4. At higher temperatures the thermodynamics becomes more complex as revealed in the published phase diagrams for the Mn – O system [8, 9].

Table 3. Characteristics of various Mn – MnO_2 reaction possibilities

		Stoichiometric composition		
Scheme	Reaction	Mn, wt %	MnO_2, wt %	$T_{adiabatic}$, K
I	$Mn + MnO_2 \rightarrow 2MnO$	38.7	61.3	2556
II	$Mn + 2MnO_2 \rightarrow Mn_3O_4$	24.0	76.0	2023
III	$Mn + 3MnO_2 \rightarrow 2Mn_2O_3$	17.4	82.6	

3.2.1 Thermal decomposition of γ-MnO_2

Thermal decomposition of the γ-MnO_2 oxidant in air and oxygen has been studied extensively by thermogravimetric analysis and other techniques [10, 11]. Reported mass loss occurs in a series of decomposition steps corresponding to the following sequence of reactions [10]:

Scheme IV:

$$\underset{1.00}{MnO_2} \xrightarrow{I} \underset{0.91}{Mn_2O_3} \xrightarrow{II} \underset{0.88}{Mn_3O_4} \xrightarrow{III} \underset{0.82}{MnO}$$

The numbers below the compounds indicate mass values relative to the starting material MnO_2. Step I is observed near 550 °C, Step II around 950 °C and Step III usually occurs above 1200 °C. The expected incremental mass losses are 9.2, 3.4 and 7.0 wt % (for product relative to immediate precursor). Figure 5 shows the TG and DSC results obtained for MnO_2 in oxygen at a scan rate of 30 °C/min. The present results are in broad agreement with these expectations except that a slightly higher mass loss was recorded in the first step. Only the onset of MnO formation is observed as the measurement temperature did not extend to temperatures above 1200 °C.

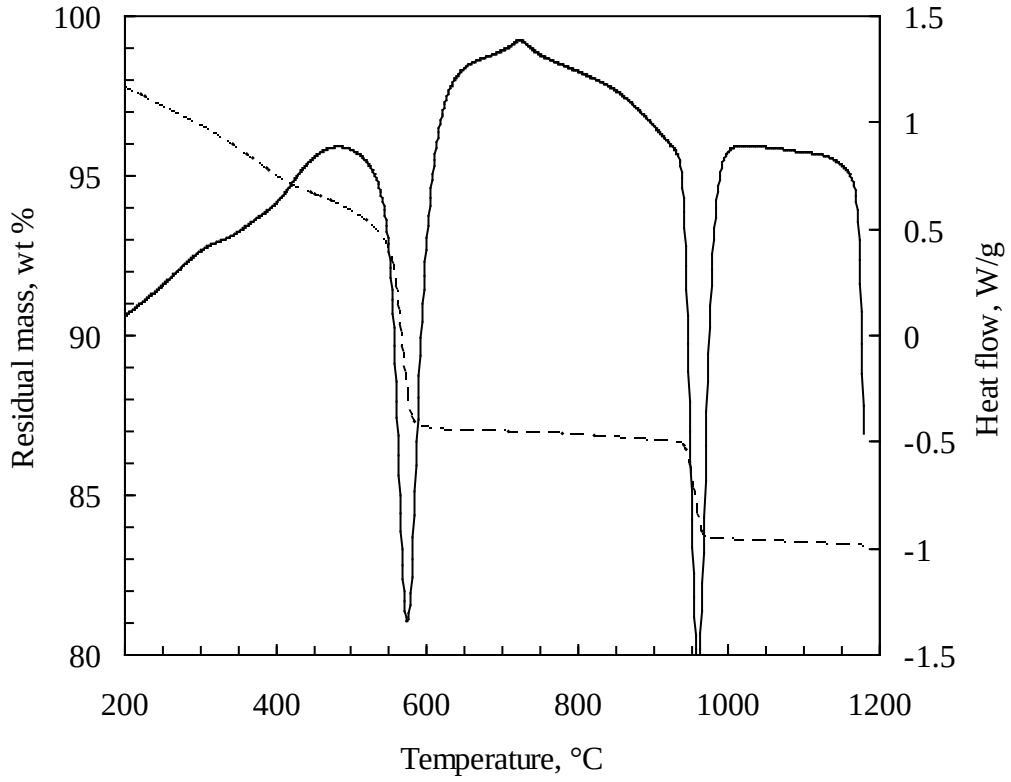

Figure 5. TG and DSC scans for MnO_2 powder heating at 30ºC/min in pure oxygen.

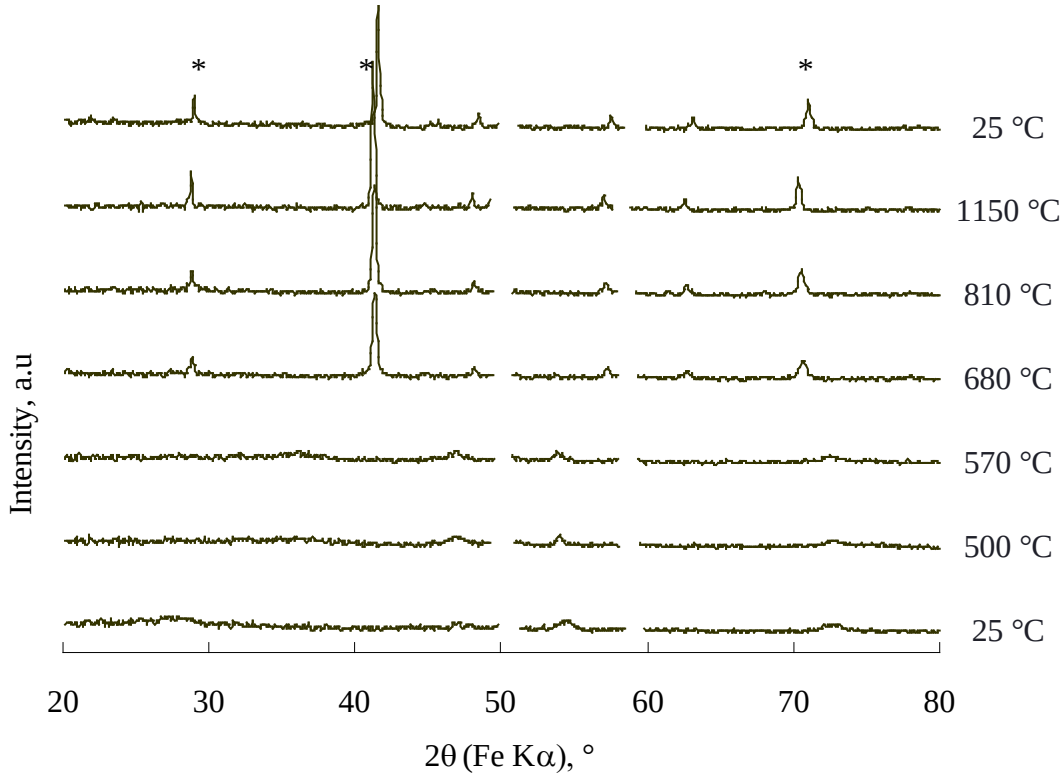

Figure 6. HTXRD scans of pure MnO_2 powder heated in static air. Key: * = Mn_2O_3.

Figure 6 shows the high temperature XRD results for MnO_2 powder heated in air. The initial scan at 25°C and those recorded at 570 °C and 680 °C show only weakly developed peaks at 36°, 52° and 74°, the expected positions characteristic peaks for MnO_2. This implies an amorphous state of the sample, probably caused by the ball milling process. The spectra recorded at higher temperatures and, also at 25°C after cooling the sample down, show peaks characteristic of Mn_2O_3 positioned at 42°, 72° and 29° in the correct order of decreasing intensity. This result differs from the observations made by Zaki *et al* [14] when studying the thermal decomposition of β-MnO_2. They found that MnO_2 underwent separate decomposition steps in air and oxygen as follows:

Scheme V:

$$\underset{1.00}{MnO_2} \xrightarrow{I} \underset{0.93}{Mn_5O_8} \xrightarrow{II} \underset{0.91}{Mn_2O_3} \xrightarrow{III} \underset{0.88}{Mn_3O_4} \xrightarrow{IV} \underset{0.82}{MnO}$$

In this case the transitions occurred at I: 650-680 °C; II: 820-830 °C and III: $Mn_2O_3 \rightarrow Mn_3O_4$ at 880-1050 °C. The present XRD results do not show the formation of either Mn_5O_8 or Mn_3O_4. The reasons for this are not understood but may be related to the fact that the starting material was amorphous. Alternatively, the soak times at each measurement temperature might have been too short to reach equilibrium with the air atmosphere.

3.2.2 Oxidation of manganese metal

Figure 7 shows the TG and DSC scans for the α-Mn fuel in an oxygen atmosphere. Mass increases steadily above 250 °C but shows an abrupt decline at ca. 950 ºC. Just before this

temperature it reaches a value of 137 wt %. The DSC scan shows at least three well-defined events with two exothermic peaks located at ca. 625 ºC and 800 ºC and an endothermic peak positioned at 950 ºC. The most plausible sequence of events is as follows:

Scheme V:

$$\underset{1.00}{Mn} \xrightarrow{I} \underset{1.29}{MnO} \xrightarrow{II} \underset{1.44}{Mn_2O_3} \xrightarrow{III} \underset{1.39}{Mn_3O_4}$$

Exothermic event I commences at ~560ºC and corresponds to the oxidation of Mn to MnO. In the next step the MnO is oxidized to Mn_2O_3. Endothermic event III is associated with a small mass loss and is attributed to reduction of Mn_2O_3 to Mn_3O_4. The TG scan shows an overall mass increase of only 34% at 1000 K. Assuming this increase is only due to oxidation, the oxide formed has a chemical composition corresponding to $MnO_{1.18}$. Manganese(II,IV) oxide has a metal/oxygen ratio of 1.33, while manganese monoxide has a ratio of 1. Thus the observed stoichiometry suggests that both MnO and Mn_3O_4 are present.

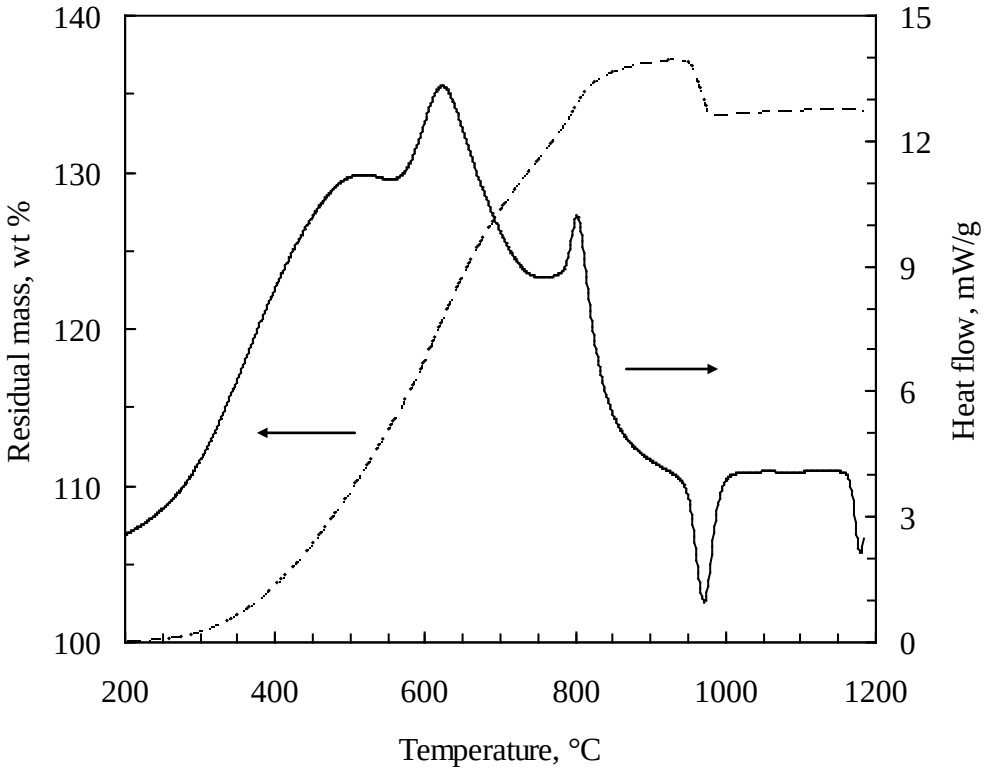

Figure 7. TG and DSC scans for manganese powder heating at 30ºC/min in pure oxygen.

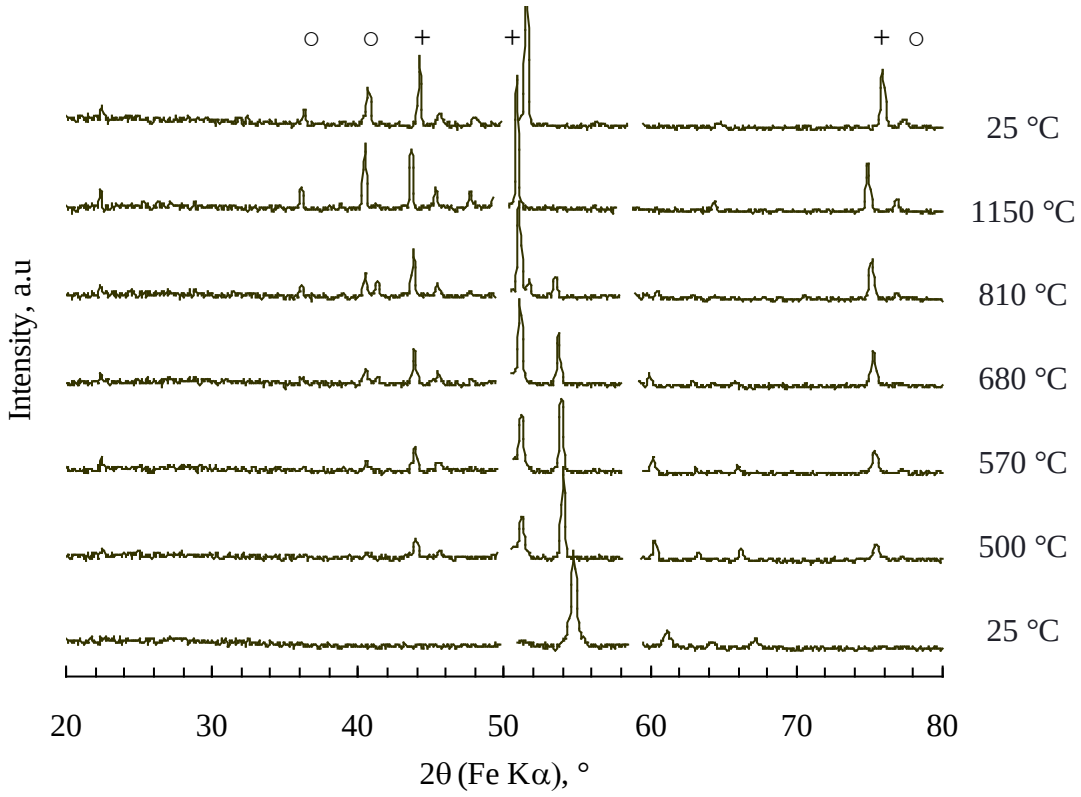

Figure 8. XRD scans of pure manganese powder heated in static air. Key: + = MnO; ○ = Mn_3O_4.

Figure 8 contains the HTXRD scan for the α-manganese powder in air. The peaks at 54° and 61°, seen in the initial scan obtained at 25°C, are characteristic for the metal. The scan at obtained at 500 °C shows three peaks located at 44°, 52° and 76° respectively. This is consistent with the oxidation of manganese to form MnO. The scan obtained at 680°C shows the appearance of an additional peak at 41° indicating the formation of Mn_3O_4. The increased intensity of the peaks at 44°, 51° and 76°, and the decreased intensity of those at 54° and 61° are consistent with progressive oxidation of the manganese. At the final measurement temperature of 1150°C, the manganese peaks have disappeared. This implies that all the manganese has been oxidized to a mixture of MnO and Mn_3O_4. This is in agreement with the DSC results in Figure 7.

3.2.3 Reaction of Mn – MnO_2 mixtures

Figure 9 displays HTXRD scans for a 50 wt % mixture of manganese and MnO_2. These scans show a number of different manganese oxides forming. The scans for 500 °C, 570 °C and 680 °C show the presence of MnO by the peaks at 44°, 52° and 76°, but by 810°C these peaks have disappeared. The scans from 570 to 1150°C show the presence of both Mn_2O_3 (peak values = 29°, 42°, 49°, 71° and 86°) and Mn_3O_4 (peaks at 22°, 36°, 41°, 45°, 55°, 65°, 75°, 84°) with Mn_2O_3 forming more rapidly than the Mn_3O_4 between 570 and 810°C, while at 1150°C the Mn_3O_4 has shown significant formation, while the Mn_2O_3 intensities have decreased.

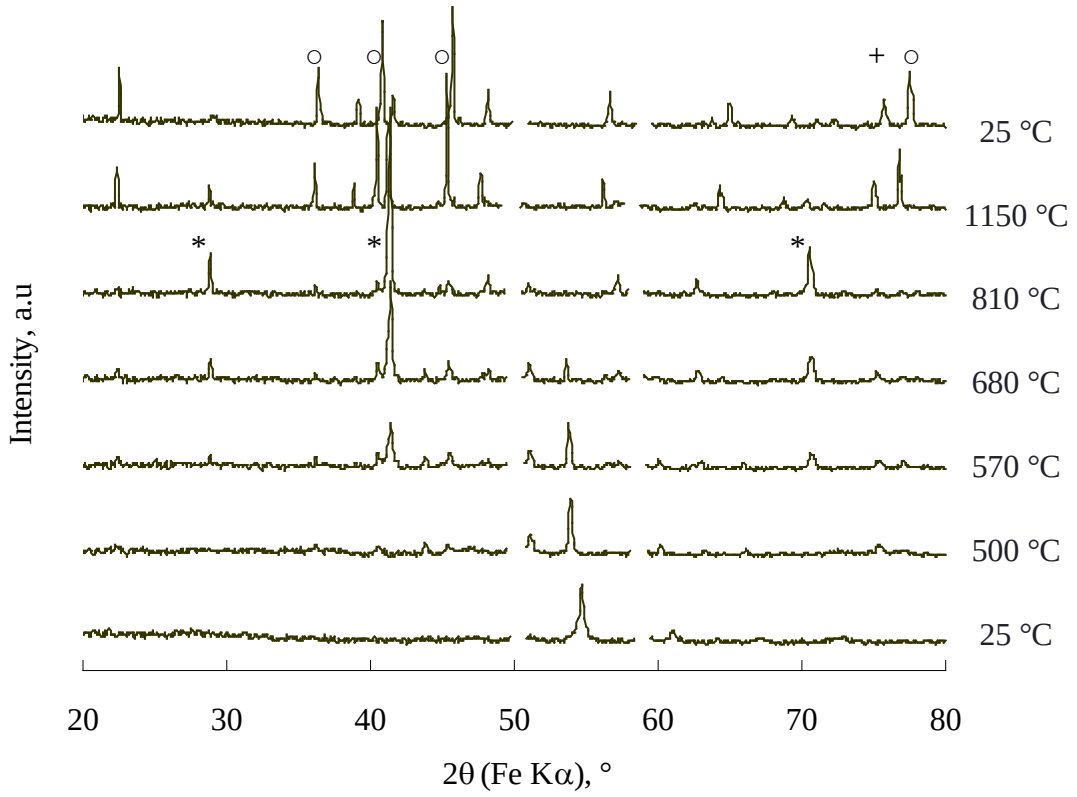

Figure 9. HTXRD scans of 50/50 (mass %) Mn/MnO_2 powder heated in static air. Key: * = Mn_2O_3; + = MnO; ○ = Mn_3O_4.

Figure 10 summarizes the compositions found for the slag residues obtained by burning the mixtures in sealed glass tubes. The composition containing 35 wt % Mn falls in between the stoichiometric compositions for the reactions corresponding to Schemes I and II in Table 3. Thus the formation of both MnO and Mn_3O_4 as reaction products is expected. This is confirmed by the results except that a small amount of Mn_2O_3 is also observed. Even though the 40 wt % Mn fuel mixture exceeds the stoichiometric requirement for MnO formation, some Mn_3O_4 is still formed. These observations imply that the reaction products do not reflect absolute equilibrium expectations. This is not surprising: Local deviations from the overall stoichiometry owing to imperfect mixing as well as kinetic factors could be responsible.

Above manganese concentrations of 40 wt %, only MnO is formed as the final oxidation product. This agrees with the reaction of Scheme I in Table 3 and the published phase diagrams [8, 9]. Since the metal fuel is in stoichiometric excess, not all of it can react. Noteworthy is the presence of β-manganese in the products for the 50, 60 and 70 wt % Mn mixtures. The temperature must have exceeded ca. 707 °C at some point in order to form this manganese phase. However, this temperature is well below the predicted adiabatic reaction temperatures.

The data in Figure 9 were obtained for force-heated samples exposed to the atmosphere. The results shown in Figure 10 are for quasi-adiabatic burning of highly compacted powders in sealed tubes. The discrepancy between these two sets of results shows that the effect of atmospheric oxygen can greatly affect the nature of the reactions that take place between manganese and MnO_2.

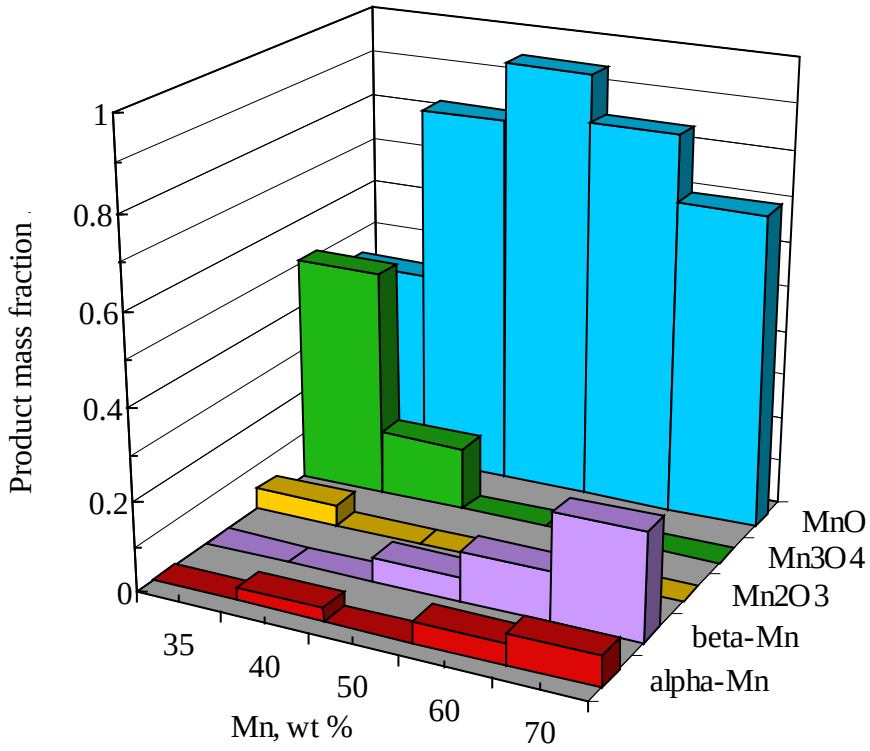

Figure 10. Product compositions obtained on burning mixtures of Mn and MnO_2 in sealed glass tubes.

4 Conclusion

Manganese metal as fuel provides for medium to slow burning pyrotechnic compositions when combined with the following oxidisers: Bi_2O_3, $CuBi_2O_4$, MnO_2, Cu_2O, V_2O_5, Sb_6O_{13} and CuO. For the mixtures pressed in aluminium tube, the reaction with Bi_2O_3 was the fastest at 22 mm/s and with Cu_2O was the slowest at ca. 5 mm/s. It was possible to decrease the burn rate to below 5 mm/s by formulating suitable multicomponent mixtures. Adding ca. 5 wt % hollow glass spheres was particularly effective in this regard.

Binary compositions based on Mn – Sb_6O_{13} and Mn – CuO burnt reliably in rolled lead tubes but not as pressed compositions in aluminium tubes. This failure is attributed to enhanced lateral heat losses via the high thermal conductivity of aluminium.

The reliable burning of Mn – MnO_2 compositions was a surprise finding. This behaviour is counter-intuitive as the fuel and the oxidant share a common metal. Thermochemical analysis showed that the stability of the various manganese oxides decreases with increase of the oxidation number of the manganese in the compound. MnO is thermodynamically the most stable oxide. It is the main product when fuel rich mixtures of Mn and MnO_2 are reacted in sealed vessels. The reaction products obtained on heating neat Mn, MnO_2 or mixtures in open vessels leads to different oxidation products. Their nature depends on the nature of the

starting materials, the gas atmosphere as well as reaction temperature. This means that conventional thermal analysis techniques that employ open crucibles and variable atmospheres do not necessarily duplicate the reaction conditions in isolated columns of burning pyrotechnics.

Acknowledgements

Financial support from the THRIP programme of the Department of Trade and Industry and the National Research Foundation as well as African Explosives Limited is gratefully acknowledged.

5 References

[1] M. A. Wilson and R. J. Hancox, Pyrotechnic Delays and Thermal Sources. *J. Pyro.*, 2001, *13*, 9-30.

[2] J. H. McLain, Pyrotechnics: From the Viewpoint of Solid State Chemistry, Franklin Institute Press, Philadelphia, Pennsylvania, 1980.

[3] J. A. Conkling, *Pyrotechnics*, In: J. I. Kroschwitz (Ed.), *Kirk-Othmer's Encyclopedia of Chemical Technology*, 4th Ed., John Wiley and Sons, New York, 1996, Vol. 20, pp. 680- 697.

[4] E. L. Charsley, C. H. Chen, T. Boddington, P. G. Laye and J. R. Pude, Differential Thermal Analysis and Temperature Profile Analysis of Pyrotechnic Delay systems: Ternary Mixtures of Silicon, Boron and Potassium Dichromate, *Thermochim. Acta*, 1980, *35*, 141-152.

[5] B. I. Khaikin and A. G. Merzhanov, Theory of Thermal Propagation of a Chemical Reaction Front. *Comb. Exp. Shock Waves*, 1966, *2*, 36-46.

[6] L. Kalombo, O. Del Fabbro, C. Conradie and W. W. Focke, Sb_6O_{13} and Bi_2O_3 as oxidants for Si in pyrotechnic time delay compositions. *Propellants, Explos., Pyrotech.*, 2007, *32*, 454-460.

[7] A. J. Tulis, Flowability Techniques in the Processing of Powdered Explosives, Propellants and Pyrotechnics. *J. Hazard. Materials*, 1980, *4*, 3-10.

[8] M. Wang, B. Sundman, Thermodynamic Assessment of the Mn-O System. *Metall. trans., B, Proces.*, 1992, *23*, 821-831.

[9] A. N. Grundy, B. Hallstedt, L. J. Gauckler, Assessment of the Mn-O System. *J. Phase Equilib.*, 2003, *24*, 21-39.

[10] B. D. Desai, J. B Fernandes, V. N. K. Dalal, *J. Power Sources*, 1985. *16*, 1-43.

[11] B. Liu, P. S. Thomas, A. S. Ray and R. P. Williams, The effect of Sampling Conditions on the Thermal Decomposition of Electrolytic Manganese Dioxide. *J. Therm. Anal. Calorim*., 2004, *76*, 115-122.

[12] C. W. Bale, E. Bélisle, P. Chartrand, S. A. Decterov, G. Eriksson, K. Hack, I.-H. Jung, Y.-B. Kang, J. Melançon, A. D. Pelton, C. Robelin and S. Petersen. FactSage Thermochemical Software and Databases - Recent Developments, *Calphad*, 2008, article in press

[13] H. J. T. Ellingham, Reducibility of Oxides and Sulfides in Metallurgical Processes, *J. Soc. Chem. Ind.*, 1944, *63*:125-133.

[14] M. I. Zaki, M. A. Hasan, L. Pasupulety, K. Kumari K. Thermochemistry of Manganese Oxides in Reactive Gas Atmospheres: Probing Redox Compositions in the Decomposition Course $MnO_2 \rightarrow MnO$. *Thermochim. Acta*, 1997, *303*, 171-181.